CrossMark

RESEARCH ARTICLE

Ion Mobility Studies on the Negative Ion-Molecule Chemistry of Isoflurane and Enflurane

Ramón González-Méndez,[1] Peter Watts,[1] David C. Howse,[1] Immacolata Procino,[2] Henry McIntyre,[2] Chris A. Mayhew[1,3]

[1]School of Physics and Astronomy, University of Birmingham, Edgbaston, Birmingham, B15 2TT, UK
[2]Smiths Detection, Century House, Maylands Avenue, Hemel Hempstead, Hertfordshire HP2 7DE, UK
[3]Institut für Atemgasanalytik, Leopold-Franzens-Universität Innsbruck, Rathausplatz 4, A-6850, Dornbirn, Austria
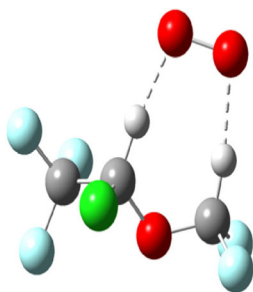
Abstract. In the present work we present an investigation of the negative ion-molecule chemistry of the anaesthetics isoflurane, ISOF, and enflurane, ENF, in an ion mobility spectrometry/mass spectrometry (IMS/MS), in both air and nitrogen. Hexachloroethane (HCE) was introduced in both air and nitrogen to produce Cl^- as a reactant ion. This study was undertaken owing to uncertainties in the chemical processes, which lead to the cluster ions reported in other work (Eiceman et al. Anal. Chem. 61, 1093–1099, 1). In particular for ISOF the product ion observed was $ISOF.Cl^-$, and it was suggested that the Cl^- was formed by dissociative electron attachment (DEA) although there was mention of a chlorine containing contaminant. We show in this study that ISOF and ENF do not produce Cl^- in an IMS system either by capture of free electrons or reaction with O_2^-. This demonstrates that the Cl^- containing ions, reported in the earlier study, must have been the result of a chlorine containing contaminant as suggested. The failure of ISOF and ENF to undergo DEA was initially surprising given the high calculated electron affinities, but further calculations showed that this was a result of the large positive vertical attachment energies (VAEs). This experimental work has been supported by electronic structure calculations at the B3LYP level, and is consistent with those obtained in a crossed electron-molecular beam two sector field mass spectrometer. An unusual observation is that the monomer complexes of ISOF and ENF with O_2^- are relatively unstable compared with the dimer complexes.

Keywords: Ion mobility spectrometry, IMS-MS, Isoflurane, Enflurane, Ion-molecule reactions

Introduction

Isoflurane (ISOF) and enflurane (ENF) are volatile halogenated ethers that are used as anaesthetics in human medicine, although their use is starting to decline and being replaced with sevoflurane. The use of ion mobility spectrometry/mass spectrometry (IMS/MS) to detect and monitor ISOF, $CF_3CHClOCHF_2$, and ENF, CHF_2OCF_2CHFCl has been reported previously [1], and a device designed for that purpose has been patented [2]. ISOF has also been proposed as a chemical standard for calibrating IMS systems [3]. Cluster ions such as $ISOF.Cl^-$ and $ENF.O_2^-$ were reported and it was suggested that the Cl^- was formed by dissociative electron attachment (DEA), although there was mention of a chlorine containing contaminant [1]. In this paper, we report a reinvestigation of this earlier work to clarify the ion chemistry involved in an IMS system. As will be seen, no Cl^- containing ions were observed in either air or nitrogen with ISOF and ENF. Hexachloroethane (HCE) was therefore introduced to produce Cl^- ions in an attempt to replicate the earlier work.

HCE has been used as a dopant in IMS for the detection of explosives [4–8]; its chemistry, however, has not been studied in depth, so a secondary aim of this present paper is a report of the results of our study of HCE.

The experimental work presented here has been supported by electronic structure calculations using the B3LYP functional and the 6-31 + G(d,p) basis set.

Correspondence to: Ramón González–Méndez;
e-mail: R.GonzalezMendez@bham.ac.uk

Experimental

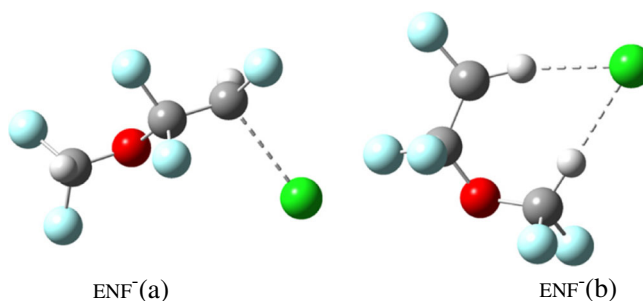### Ion Mobility Spectrometry-Mass Spectrometry (IMS/MS)

IMS is a gas-phase analytical instrument used to temporally separate reactant and product ions in a drift tube according to their mobility [9]. The IMS/MS system used in this study has been described elsewhere [10–14]. In brief, the instrument consists of two drift tube regions, each 10 cm in length. The first, the reaction region containing a cylindrical radioactive ion source (nominal 10 mCi ^{63}Ni foil), is physically separated from the second region, the drift region, by a Bradbury-Nielsen (B-N) gate. A forward flow of the buffer gas flows through the radioactive source and into the glass jacket towards the B-N grid, and in this forward flow the analyte to be investigated is introduced. A contraflow of the same buffer gas is introduced through apertures near to a Faraday plate (FP). Typical forward and contraflows are 0.4 L min^{-1} and 0.8 L min^{-1} (at slightly above the ambient atmospheric pressure and room temperature), respectively. These flows are controlled by mass flow controllers (Alicat, ±1% accuracy). The two flows are vented out of the drift tube through holes in the B-N ring. The drift tube's pressure is measured with a strain gauge absolute pressure sensor (Edwards, model ASG 2000). A thermocouple is used to monitor the temperature of the buffer gas near to the exhaust region. The temperature of the drift tube is electronically controlled at a constant temperature of 30 ± 1 °C to avoid the need to compensate for changes in ambient temperature. An electric field along the axis of the drift tube is set at 200 V·cm^{-1} by applying a suitable voltage gradient across the whole of the drift tube.

The FP is protected by a screen grid to shield it from the electric field produced by the oncoming ion swarm. At the center of the FP there is a 0.07 mm pinhole, separating the IMS from the lower pressure quadrupole mass spectrometer region. The product ions are separated according to their m/z values using quadrupole mass filter and detected using a secondary electron multiplier. For this identification of the m/z values, the B-N grid in the drift tube is kept open in order to maximize ion signal intensity.

To obtain ion mobility spectra, the B-N gate is used to pulse reactant and product ions generated in the reaction region into the drift region at a frequency of 25 Hz and a pulse width of 600 μs (600 μs was necessary because at shorter pulse widths the ion signals associated with isoflurane and enflurane were significantly weaker, presumably owing to the transit times of the product ions

ENF$^-$(a)   ENF$^-$(b)

Figure 1. Structure of two possible negative ENF ions obtained from DFT calculations

through the B-N grid). Mobility spectra were acquired by means of intentionaly written software using Labview [14]. Total ion mobility spectra were acquired using the FP. Tuned ion mobility spectra were obtained by sampling ions through the FP and then allowing a specific m/z through the mass filter. The tuned ion mobility spectra were used to verify contributions of product ions to the individual peaks in the total ion mobility spectra.

Procedures and Chemicals

Isoflurane and hexachloroethane were purchased from Sigma Aldrich (UK), both with stated purities of 99%. Enflurane was purchased from Fluorchem Ltd. (UK) with a stated purity of 97%. All chemicals were used without further purification. At room temperature isoflurane and enflurane are liquids and hexachloroethane is a white granulated solid. For the liquid samples, typically 50 μL were spotted onto cotton placed inside a glass syringe (Weber Scientific, UK), which was inserted through a septum into the forward flow. A syringe driver (Cole Palmer 74900 series; IL, USA) was used to introduce the compound into the forward flow at a constant rate. For hexachloroethane, a few mg were deposited into a glass vial sealed with a PTFE septum (Thames Restek, Bellefonte, PA, USA) through which the forward gas flowed.

Zero air grade and pure nitrogen (oxygen free and 99.998% minimum nitrogen) carrier gases used for this experiment were purchased from BOC Gases (UK). Prior to entering the reaction region, all carrier gases were passed through moisture and hydrocarbon traps (Supelco 23991 and Agilent BHT-4, respectively).

DFT Calculations

These were conducted using Gaussian09W and GaussView05 for Windows [15]. All calculations used the B3LYP hybrid functional and (unless stated otherwise) the 6-31 + G(d,p) basis
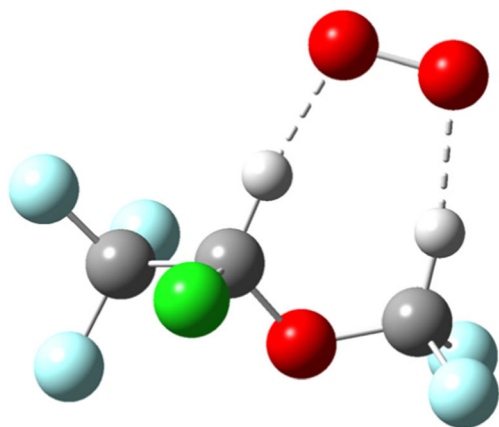
Table 1. Dependence of EA and VAE in kJ·mol^{-1} upon Basis Set Using the B3LYP Functional at 298 K. In the VAE Column the Figures in Parentheses are the Number of Imaginary Frequencies Observed

Basis set	EA kJ·mol^{-1}	VAE kJ·mol^{-1}
6-31 + G(d,p)	170	+60 (4)
6-31++G(d,p)	170	+39 (3)
6-31 + G(3df,2p)	154	+60 (3)
6-31++G(3df,2p)	154	+45 (1)
6-31 + G(2d,2p)	161	+62 (3)
6-311++G(3df,2p)	156	+45 (1)
6-31G(d,p)	109	+182 (3)

Table 2. ΔHs and ΔGs for the Possible Reactions of ISOF in Air. DFT Calculations Were Performed Using the B3LYP Functional and the 6-31 + G (d,p) Basis Set

Reactants	Ionic products	ΔH_{298} kJ·mol^{-1}	ΔG_{298} kJ·mol^{-1}
ISOF + e	ISOF$^-$	−170	−183
	CHF$_2$OCHCF$_3$ + Cl$^-$	−65	−106
ISOF + O$_2^-$	ISOF$^-$ + O$_2$	−110	−124
	ISOF$^-$.O$_2$	−146	−111
ISOF$^-$.O$_2$ + ISOF	ISOF$_2^-$.O$_2$	−92	−51
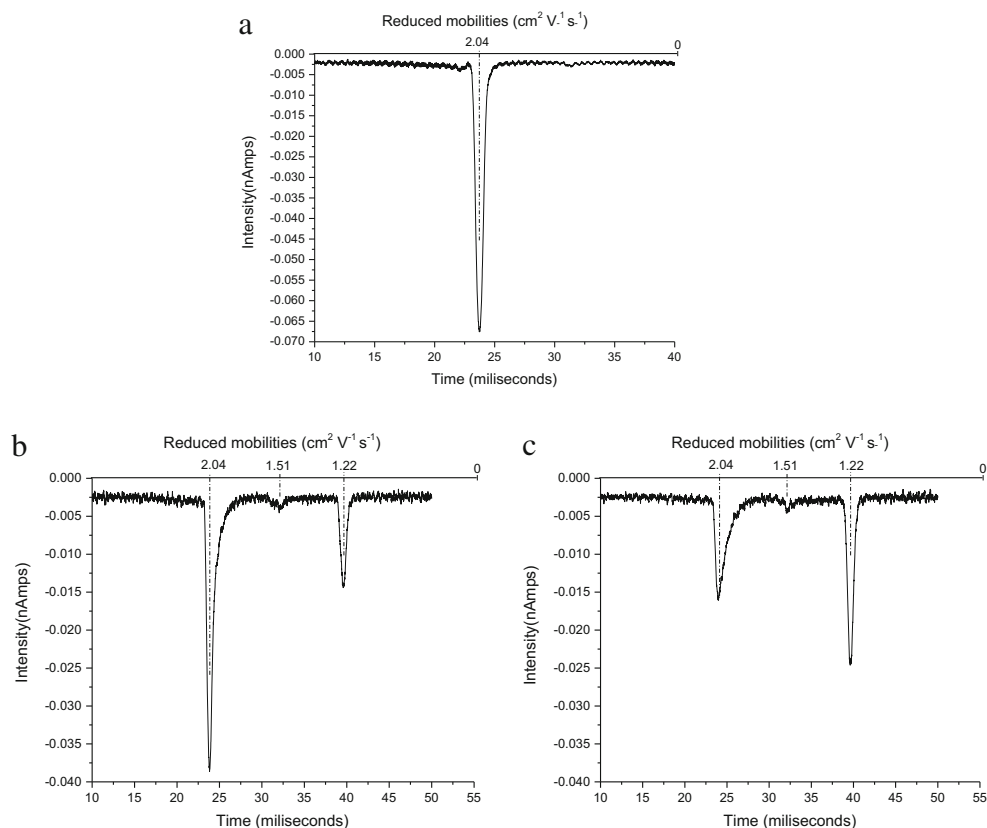
Figure 2. IMS spectra showing (**a**) the air RIP and air doped with ISOF showing the air RIP, ISOF.O_2^- and (ISOF)$_2$.O_2^- peaks for two ISOF concentrations (**b**) lower and (**c**) higher

set. We have found this combination to give fair agreement with published values of the adiabatic electron affinities of species such as Cl and O_2 and 1,3,5-trinitrobenzene and reactions such as OH$^-$ with H$^+$ and Cl$^-$ with H$^+$ [16]. Stable species were characterized by the absence of an imaginary frequency. Adiabatic electron affinities (AEAs) were determined by calculating the total energy of an anion at its optimized geometry and subtracting from this the total energy of the neutral at its optimized geometry. Vertical attachment energies (VAE) correspond to the change in energy on attachment of an electron to the ground state of a molecule without any change of nuclear

geometry. These were determined by doing a frequency calculation after placing a negative charge on the ground state geometry of the neutral and then subtracting the computed total energy of the neutral from that of the anion.

Results and Discussion

Electron Attachment

ISOF Despite both electron attachment (EA) and dissociative electron attachment (DEA) being calculated thermodynamically favorable, adiabatic EA 1.76 eV (170 kJ mol^{-1}) and DEA to yield Cl$^-$ $\Delta H_{298} = -65$ kJ mol^{-1} and $\Delta G_{298} = -106$ kJ mol^{-1}, neither was observed with near-thermal electrons in nitrogen.

Figure 3. Structure for the stable monomer ISOF.O_2^- from DFT calculations

Table 3. ΔHs and ΔGs for the Reaction of ENF in air. DFT Calculations Were Performed Using the B3LYP Functional and the 6-31 + G (d,p) Basis Set

Reactants	Products	ΔH_{298} kJ·mol^{-1}	ΔG_{298} kJ·mol^{-1}
ENF + e	ENF$^-$(a)	−104	−115
	ENF$^-$(b)	−146	−154
	CHF$_2$OCF$_2$CHF + Cl$^-$	−52	−93
ENF + O_2^-	ENF–(a) + O_2	−44	−55
	ENF–(b) + O_2	−86	−94
	ENF.O_2–(a)	−87	−45
	ENF.O_2–(b)	−96	−62
	ENF.O_2–(c)	−138	−101
ENF.O_2^-(c) + ENF	ENF$_2$.O_2–(a)	−83	−41
	ENF$_2$.O_2–(b)	−56	−20
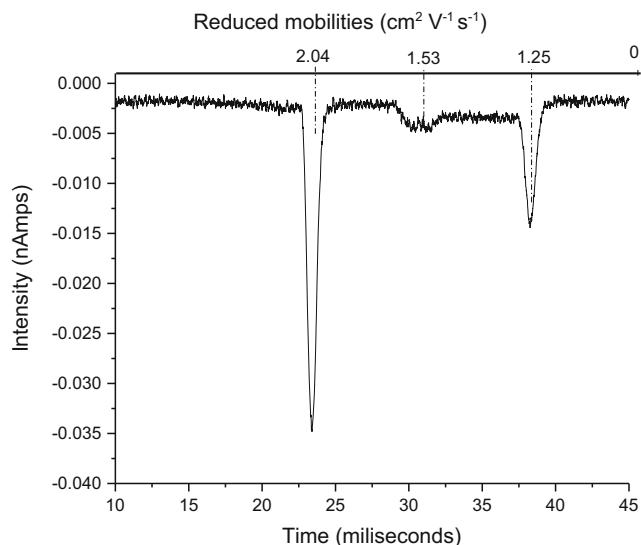
Figure 4. IMS spectrum after adding sufficient ENF to decrease the air RIP by about 50%

Table 4. ΔHs and ΔGs for the DEA of HCE. DFT Calculations Were Performed Using the B3LYP Functional and the 6-31 + G (d,p) Basis Set

Reactants	Ionic products	ΔH_{298} kJ·mol^{-1}	ΔG_{298} kJ·mol^{-1}
HCE + e	Cl$^-$	−122	−170
	Cl$_2^-$	−215	−275
HCE + O$_2^-$	Cl$^-$	−62	−110
	Cl$_2^-$	−152	−216

This suggests that the VAE is positive. As calculated VAEs, given in Table 1, and adiabatic EAs are basis set-dependent, the influence of basis set was briefly investigated using the B3LYP functional [17–19]. A representation of the structure of the anion ISOF$^-$ derived from DFT calculations is shown in Supplementary Figure S1.

The influence of the basis set shows a different pattern for the EA and VAE. The most important feature of the basis set is to have a diffuse function – increasing this from + to ++ has no effect upon the EA but causes a decrease in the VAE. Increasing the polarization functions from (d,p) to (3df,2p) has a small effect upon the EA but not upon the VAE. Going from 6-31 to 6-311 has no effect upon either, at least with the diffuse and polarization functions used. Overall, so long as both polarization and diffuse functions are included, the calculated EA and VAE are of sufficient accuracy to allow the identification of trends and to arrive at an understanding of the experimental observations.

Inspection of the imaginary frequencies in the VAE calculations showed that even when there were multiple

imaginary frequencies, one was always dominant (i.e., was considerably more intense than other imaginary frequencies), and was associated with stretching of the C–Cl bond. IRC Intrinsic reaction coordinate (IRC) calculations were used to follow the C–Cl stretch and showed that the initial structure associated with the VAE relaxed to the structure found in the calculation of the adiabatic EA. It is suggested that the non-observation of attachment of thermal electrons is the result of a VAE of ca. +60 kJ·mol^{-1} (0.62 eV). This is in excellent agreement with a resonance of 0.6 eV leading to Cl$^-$ observed in a recent study of DEA of ENF, ISOF, and HCE in a crossed electron-molecular beam two sector field mass spectrometer [20].

ENF ENF is a little more complicated than ISOF as calculations show that there are two stable negative ions denoted ENF$^-$(a) and ENF$^-$(b) in the structures (Figure 1). ENF has an effective EA of 104 kJ·mol^{-1} (1.08 eV) when forming ENF$^-$(a) and an effective EA of 146 kJ·mol^{-1} (1.51 eV) when forming ENF$^-$(b). DEA is thermodynamically favorable with $\Delta H_{298} = -65$ kJ·mol^{-1} and $\Delta G_{298} = -106$ kJ·mol^{-1}. However, as seen earlier for ISOF, neither EA nor DEA is observed. The VAE is calculated (using 6-31 + G(d,p)) to be +74 kJ·mol^{-1} (0.77 eV) with four imaginary frequencies. An IRC calculation on this species shows it relaxing to give ENF$^-$(a).

Attempts were made to find a transition state between ENF$^-$(a) and ENF$^-$(b) but these were unsuccessful. Various relaxed scans of bond lengths and dihedral angles were investigated on the structure of ENF$^-$(a) and numerous stable configurations differing by only a few kJ·mol^{-1} were found, and when one approached close to ENF$^-$(b) it just flicked over with no discernible transition state.
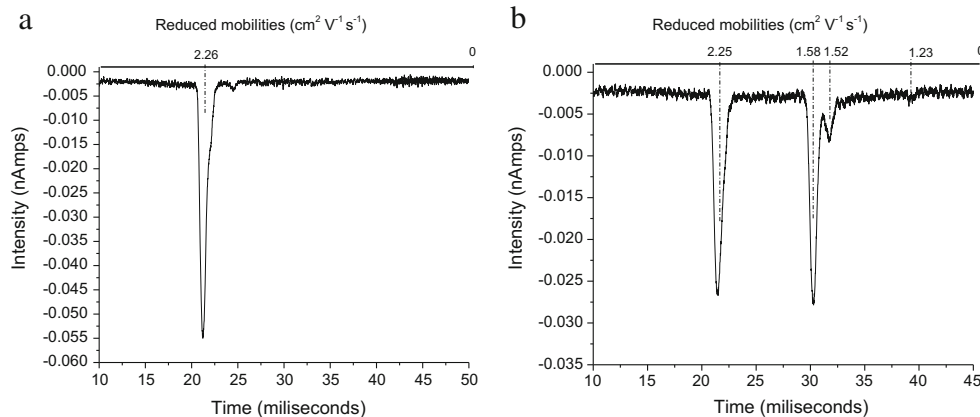

Figure 5. IMS spectra of (a) air doped with HCE and (b) after introducing a small amount of ISOF

Table 5. ΔHs and ΔGs for the Possible Reactions of ISOF and HCE in Air. DFT Calculations were Performed Using the B3LYP Functional and the 6-31 + G (d,p) Basis Set

| Reactants	Ionic products	ΔH_{298} kJ·mol^{-1}	ΔG_{298} kJ·mol^{-1}
ISOF + Cl$^-$	ISOF.Cl$^-$	−108	−79
ISOF.Cl$^-$ + ISOF	ISOF$_2$.Cl$^-$	−74	−40
ISOF + Cl$_2^-$	ISOF.Cl$_2^-$	−75	−44
ISOF.Cl$_2^-$ + ISOF	ISOF$_2$.Cl$_2^-$	−58	−2

Reactions in Air

ISOF Although thermodynamically feasible (see Table 2), neither electron transfer nor dissociative electron transfer from O_2^- is observed. Neither is proton abstraction; only complexation with O_2^- occurs.

The air reactant ion peak (RIP) is initially sharp and reasonably symmetrical (see Figure 2a). It is appreciated that the air RIP is a complex with the O_2^- ions being complexed to varying degrees with O_2, H_2O, and CO_2, and that the degree of complexation varies during the migration of the ions down the reaction region (for a detailed description of the air RIP see Hayhurst et al. [21] and Watts [22]). But as only complexation with O_2^- is observed, discussion of the potential complexation with other negative RIP ions will not be considered further.

Addition of sufficient ISOF to decrease the RIP by 50% shows a good dimer peak ((ISOF)$_2$.O_2^-), and a small monomer (ISOF.O_2^-) [Neither structural information nor charge distribution is implied when identifying an ion in this form]. (see Figure 2b and c). Broadening of the RIP on the low mobility side is observed. This is consistent with an unstable monomer complex being formed, which can either rearrange to give a stable monomer or which can decompose to give O_2^- related ions to broaden the RIP. The monomer can react with more ISOF to give a stable dimer (ISOF)$_2$.O_2^-. DFT calculations show that there is only one stable monomer, the structure of which is shown below (Figure 3) and the energetics provided in Table 2.

A search for less stable complex(es) of ISOF and O_2^- was made. No minima were found, suggesting that the potential energy surface is relatively flat.
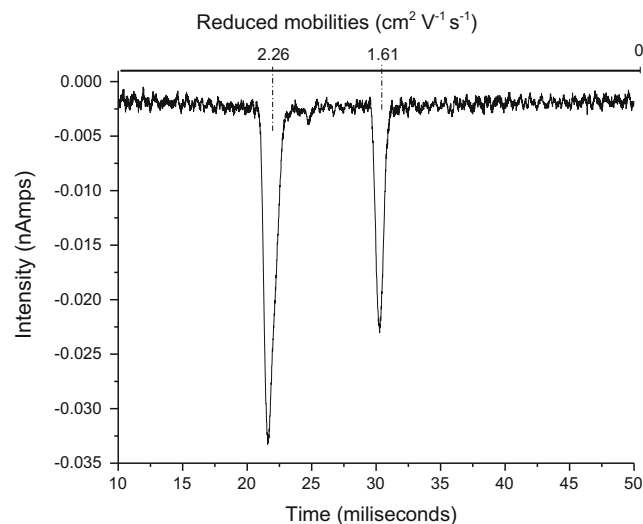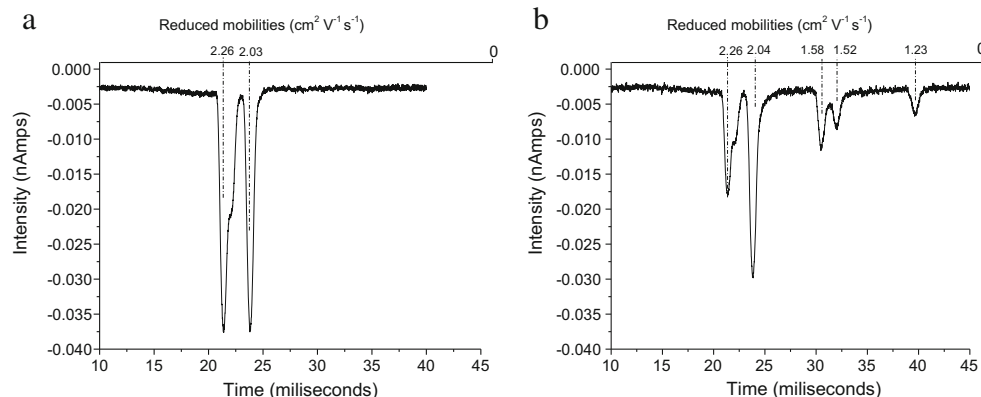

Figure 7. IMS spectrum of air doped with HCE with the addition of ENF

The number of possible structures of the dimer anion is greater than the two shown in Supplementary Figure S2 as both ISOF and ENF are chiral and are sold as racemic mixtures and, thus, for any possible dimer structure there are two sub-structures either both molecules having the same configuration (i.e., R + R or S + S) or different configurations (i.e., R + S). A selection has been investigated, but as each ISOF is acting as a bidentate ligand (to give slightly puckered 7-membered rings) in the dimer they all have similar energies.

ENF As with ISOF, although thermodynamically feasible, neither electron transfer nor dissociative electron transfer from O_2^- is observed, see Table 3.

Addition of sufficient ENF to reduce the air RIP by ca. 50% gave a good dimer peak bridging (i.e., with an elevated baseline indicating decomposition of the dimer to the monomer, to a small monomer). Unlike with ISOF, no broadening of the RIP is observed (see Figure 4).

In contrast to ISOF, three stable structures for the monomer ENF.O_2^- have been found and are shown in Supplementary Figure S3. Whilst transition states (TS) between these three ENF.O_2^- monomer structures have yet to be found, it is likely

Figure 6. IMS spectra of air doped with enough HCE to (**a**) have similar intensities of air RIP and HCE RIP, (**b**) to have similar amounts of air RIP and HCE RIP with the addition of sufficient ISOF to decrease the HCE RIP by about 50%

Table 6. ΔHs and ΔGs for the Reaction of ENF with the HCE RIP. DFT Calculations Were Performed Using the B3LYP Functional and the 6-31 + G (d,p) Basis Set

Reactants	Products	ΔH_{298} kJ·mol^{-1}	ΔG_{298} kJ·mol^{-1}
$ENF + Cl^-$	$ENF.Cl^-$	−104	−70
$ENF + Cl_2^-$	$ENF.Cl_2^-$	−68	−25
$ENF.Cl^- + ENF$	$ENF_2.Cl^-$	−66	−33

that the TS energies will be small and that the energies for the formation of the complexes $ENF.O_2^-$ [(a) and (b)] will be sufficient to overcome them, leading to $ENF.O_2^-$(c) being the only stable monomer observed—this has a similar structure to that shown for $ISOF.O_2^-$ in Figure 3. As the monomer peak is small and the RIP has not broadened, this suggests that initial complexes of $ENF.O_2^-$ are so unstable that they decompose sufficiently rapidly that the reformed O_2^- ions are encompassed in the RIP.

The formation and structures of the dimer $(ENF)_2.O_2^-$ is more complex than was found for the case with ISOF. Several structures (many if the formation of a dimer from $ENF.O_2^-$[(a) and (b)] are considered) of a dimer from $ENF.O_2^-$ (c) are possible, but only two have negative ΔGs of formation. These are shown in Supplementary Figure S4.

The sharp dimer peak at $K_o = 1.25$ cm^2·V^{-1}·s^{-1} shown in Figure 4 is assigned to $(ENF)_2.O_2^-$(a). The unstable dimer anion causing the bridging between the monomer and dimer anions and the broadening of the monomer is therefore assigned as $(ENF)_2.O_2^-$(b). The lower stability of the cyclic complexes containing O_2^- compared with the corresponding complexes of ISOF is to be expected as the former forms an 8-membered ring whereas ISOF only requires a 7-membered ring.

Reactions in Air Doped with Hexachloroethane (HCE)

On addition of HCE to an air system, a more mobile RIP is produced consisting of a sharp peak (Cl$^-$ related ions) with a trace of a shoulder on the less mobile side (Cl$_2^-$) – see Figure 5a. A

similar RIP is also seen on introduction of HCE into a nitrogen system. This is to be expected as the calculated VAE is −33 kJ mol^{-1} and the overall thermodynamics are favorable – see Table 4.

ISOF Addition of ISOF to an air system doped with HCE (similar to the one shown in Figure 5a), shows two peaks, $ISOF.Cl^-$ and $ISOF.Cl_2^-$ together with a suggestion of an unstable dimer $(ISOF)_2.Cl^-$, (Figure 5b. $ISOF.Cl_2^-$ does not form a dimer. These observations are in agreement with the thermodynamics given in Table 5. The structures of the Cl$^-$ and Cl$_2^-$ complexes with ISOF are similar to those with O_2^- when the O_2^- is acting as a bidentate ligand (i.e., forms a ring).

It was observed that the air system was much less sensitive to ISOF than was the HCE system. In order to verify this, sufficient HCE was introduced into an air system to give an approximately 50/50 mix of air and HCE RIPs, as seen in Figure 6a.

What is immediately apparent is that the Cl$_2^-$ contribution to the HCE RIP appears to be much greater than in Figure 2b and c. Addition of ISOF gives three product peaks $ISOF.Cl^-$, $ISOF.Cl_2^-$, and $(ISOF)_2.O_2^-$ (see Figure 6b), thus confirming the observation of the high sensitivity to ISOF in a doped system compared with an undoped system.

The suggestion that more Cl$_2^-$ is formed in a partially doped system is confirmed by the changing ratio of $ISOF.Cl^-$ to $ISOF.Cl_2^-$ in Figure 5b and Figure 6b. Why should this be? On full doping, HCE dominates the electron capture but on partial doping oxygen competes successfully for electrons. The reaction of O_2^- with HCE favors the production of Cl$_2^-$ over Cl$^-$.Mass spectra data show that in the 50/50 system the ratio of Cl$^-$/Cl$_2^-$ is ca. 3.5, whereas in a normally doped system (sufficient HCE to remove the air RIP) the ratio is ca. 5.2. Increasing the HCE concentration much higher leads to a ratio of ca. 19, similar to that in nitrogen. The ratio in nitrogen is insensitive to the HCE concentration.

As the DEA to yield Cl$_2^-$ is energetically more favorable than that yielding Cl$^-$, it might be expected that it would be the dominant pathway. However, since DEA to yield Cl$^-$ is energetically favorable and can occur with any conformation of HCE, it may be that the Cl$_2^-$ can only be formed when the
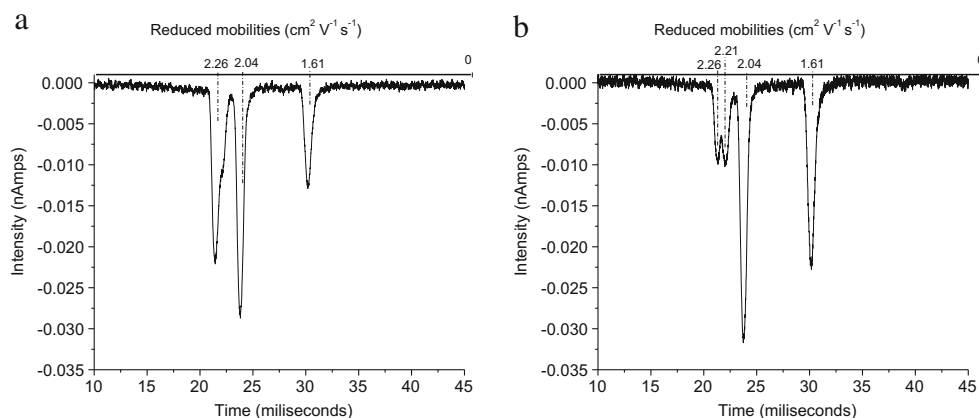
Figure 8. IMS spectra of air doped with enough HCE to have similar amounts of air RIP and HCE RIP after introducing a small amount of ENF (**a**) and a higher amount of ENF (**b**)

chlorines in the HCE are in the unstable eclipsed conformation, thus accounting for its low abundance. It is suggested that as well as direct dissociative electron transfer (DET from O_2^- to HCE to give a similar Cl^-/Cl_2^- as in DEA, a transient complex of HCE and O_2^- is formed in which the chlorines are in a more eclipsed conformation, thus leading to more Cl_2^- being formed.

ENF Only ENF.Cl^- is observed – see Figure 7. This is consistent with the energetics given in Table 6. Again, the strain of an 8-membered ring compared with a 7-membered ring accounts for the instability of the complex with Cl_2^-.

Again, it was subjectively observed that the air system was much less responsive to ENF than was the HCE system. Using the approach outlined for ISOF, the relative sensitivity to ENF in an air and HCE system was investigated – see Figure 8. When sufficient ENF to deplete the HCE peak by 50% was added, no appreciable diminution of the air RIP occurred. Increasing the ENF concentration to virtually remove the Cl^- RIP leaving just the Cl_2^- peak caused a small diminution of the air RIP with a corresponding trace of the dimer. A serendipitous experiment occurred when at the end of an air/ENF experiment the system was allowed to diminish the ENF concentration and return to a good air RIP. On addition of HCE, a strong ENF.Cl^- peak appeared.

Conclusions

ENF and ISOF do not produce Cl^- in an IMS system by capture of free electrons or reaction with O_2^-. This demonstrates that the Cl^- containing ions reported in the earlier study were the result of a chlorine containing contaminant as suggested [1]. The failure of ENF and ISOF to undergo DEA was initially surprising given the high calculated electron affinities, but further calculations showed that this was a result of the large positive VAEs. The present data are consistent with those of Matias et al. in their crossed electron-molecular beam two sector field mass spectrometer [20]. An unusual observation is that the observed monomer complexes of ISOF and ENF with O_2^- are relatively unstable compared with the dimer complexes. This is in contrast to the more usual observation that monomer complexes are more stable than dimer complexes as shown, for example, with the Cl^- complexes of ISOF and ENF. DFT calculations do show that stable complexes of ISOF and ENF with O_2^- are possible and are the likely precursors of the dimer complexes. That they are not seen is a consequence of the initial complexes being unstable, and conformational changes leading to ring formation (7 and 8, respectively, for ISOF and ENF) are required to form the stable monomer. The instability of the initial complexes require a high concentration of ISOF and ENF for them to be formed in appreciable amounts and thus the stable monomers, once formed, immediately react to form the dimers. This is consistent with the observed low sensitivity of an oxygen-based system to ISOF and ENF. Dissociative electron attachment to HCE produces primarily Cl^- with a small amount of Cl_2^-, whereas electron transfer from O_2^- gives much more Cl_2^-. It

is suggested that Cl^- can be produced from any conformation of HCE, whereas Cl_2^- can only be produced from at least a partially eclipsed conformation and that reaction with O_2^- promotes this through a transient complex with HCE.

Acknowledgements

Open Access

References

1. Eiceman, G.A., Shoff, D.B., Harden, C.S., Snyder, A.P., Martinez, P.M., Fleischer, M.E., Watkins, M.L.: Ion mobility spectrometry of halothane, enflurane, and isoflurane anesthetics in air and respired gases. Anal. Chem. **61**(10), 1093–1099 (1989)
2. Sacristan, E.: Ion mobility method and device for gas analysis. U.S. Patent No. 5,455,417. 3 Oct. (1995)
3. McIntyre, H., Thathapudi, N., Arnold, P.: Chemical calibration process, system, and device. WO 2015173579 A1, Nov. 19 (2015)
4. Puton, J., Nousiainen, M., Sillanpää, M.: Ion mobility spectrometers with doped gases. Talanta **76**(5), 978–987 (2008)
5. Ewing, R.G., Atkinson, D.A., Eiceman, G.A., Ewing, G.J.: A critical review of ion mobility spectrometry for the detection of explosives and explosive related compounds. Talanta **54**(3), 515–529 (2001)
6. Spangler, G.E., Carrico, J.P., Campbell, D.N.: Recent advances in ion mobility spectrometry for explosives vapor detection. J. Test Eval. **13**(3), 234–240 (1985)
7. Kozole, J., Levine, L.A., Tomlinson-Phillips, J., Stairs, J.R.: Gas phase ion chemistry of an ion mobility spectrometry based explosive trace detector elucidated by tandem mass spectrometry. Talanta **140**, 10–19 (2015)
8. Li, G., Zhang, Z., Huang, Q., Guo, T., Zhang, X.: A novel pulsed doping method for enhancing the sensitivity of ion mobility spectrum (iMS) for detecting explosives and a mechanism study. Sensor Lett. **13**(9), 778–784 (2015)
9. Eiceman, G.A., Karpas, Z., Hill, H.H. Jr.: Ion mobility spectrometry. CRC Press: Boca Raton, Florida (2013)
10. Liu, Y., Mayhew, C.A., Peverall, R.: A new experimental approach to investigate the kinetics of low energy electron attachment reactions. Int. J. Mass Spectrom. Ion Process **152**(2), 225–242 (1996)
11. Jarvis, G.K., Peverall, R., Mayhew, C.A.: A novel use of an ion-mobility mass spectrometer for the investigation of electron attachment to molecules. J. Phys. B Atomic Mol. Opt Phys. **29**(19), L713 (1996)
12. Jarvis, G.K., Mayhew, C.A., Singleton, L., Spyrou, S.M.: An investigation of electron attachment to $CHCl_2F$, $CHClF_2$, and CHF_3 using an electron-swarm mass spectrometric technique. Int. J. Mass Spectrom. Ion Process **164**(3), 207–223 (1997)
13. Bell, A., Giles, K., Moody, S., Watts, P.: Studies on gas-phase positive ion-molecule reactions of relevance to ion mobility spectrometry. The

reactions of 2-methyl-2-propanol (t-butyl alcohol) with protonated water clusters in an ion mobility system. Int. J. Mass Spectrom. Ion Processes **17**(1), 65–70 (1998)

14. Howse, D.C.: Development and application of an ion mobility spectometer-quadrupole mass spectometer instrument. PhD, University of Birmingham (2015)

15. Frisch, M., Trucks, G., Schlegel, H., Scuseria, G., Robb, M., Cheeseman, J., Scalmani, G., Barone, V., Mennucci, B., Petersson, G.: Gaussian 09, rev. A. 1. Gaussian Inc., Wallingford (2009)

16. Linstrom, P.J., W. G. M., (eds.) NIST Chemistry WebBook, NIST Standard Reference Database Number 69. National Institute of Standards and Technology, Gaithersburg. http://webbook.nist.gov. (2015)

17. Falcetta, M.F., Jordan, K.D.: Assignments of the temporary anion states of the chloromethanes. J. Phys. Chem. **94**(15), 5666–5669 (1990)

18. Aflatooni, K., Gallup, G.A., Burrow, P.D.: Temporary anion states of dichloroalkanes and selected polychloroalkanes. J. Phys. Chem. A **104**(31), 7359–7369 (2000)

19. Rienstra-Kiracofe, J.C., Tschumper, G.S., Schaefer, H.F., Nandi, S., Ellison, G.B.: Atomic and molecular electron affinities: photoelectron experiments and theoretical computations. Chem. Rev. **102**(1), 231–282 (2002)

20. Matias, C., Mauracher, A., Huber, S.E., Denifl, S., Limão-Vieira, P., Scheier, P., Märk, T.D., González-Méndez, R., Mayhew, C.A.: Dissociative electron attachment to the volatile anaesthetics enflurane and isoflurane and the chlorinated ethanes pentachloroethane and hexachloroethane. Int. J. Mass Spectrom. **379**, 179–186 (2015)

21. Hayhurst, C.J., Watts, P., Wilders, A.: Studies on gas-phase negative ion/molecule reactions of relevance to ion mobility spectrometry: mass analysis and ion identification of the negative reactant ion peak in "clean" air. Int. J. Mass Spectrom. Ion Process **121**(1/2), 127–139 (1992)

22. Watts, P.: Studies on gas-phase negative ion/molecule reactions of relevance to ion mobility spectrometry: kinetic modeling of the reactions occuring in "clean" air. Int. J. Mass Spectrom. Ion Process **121**(1/2), 141–158 (1992)